

Far-Ultraviolet Imaging of Jupiter's Aurora and the Io "Footprint"

John T. Clarke,* Gilda E. Ballester, John Trauger, Robin Evans, J. E. P. Connerney, Karl Stapelfeldt, David Crisp, Paul D. Feldman, Christopher J. Burrows, Stefano Casertano, John S. Gallagher III, Richard E. Griffiths, J. Jeff Hester, John G. Hoessel, Jon A. Holtzman, John E. Krist, Vikki Meadows, Jeremy R. Mould, Paul A. Scowen, Alan M. Watson, James A. Westphal

Far-ultraviolet images of Jupiter from the Hubble Space Telescope Wide Field Planetary Camera 2 reveal polar auroral emissions at 300 kilometer resolution and three times higher sensitivity than previously achieved. Persistent features include a main oval containing most of the emission and magnetically connected to the middle magnetosphere, diffuse and variable emissions poleward of the main oval, and discrete emission from Io's magnetic footprint equatorward of the oval. The auroral emissions are variable, exhibit magnetic conjugacy, and are visible above the planet limb. All emissions approximately co-rotate with Jupiter except the Io "footprint," which is fixed along Io's magnetic flux tube.

The presence and approximate strength of Jupiter's magnetic field have been known since the 1954 detection of radio emissions from trapped charged particles (1). In 1964 the decametric emissions were found to be modulated by the orbital location of Jupiter's satellite Io (2). This modulation was attributed to the electromagnetic interaction of Jupiter's magnetic field with Io, implying a $\sim 10^6$ A electric current system along magnetic field lines linking Io with Jupiter's ionosphere (3) (hereafter Io flux tube, or IFT). From the strength of the decametric emission and the implied magnetic field, Jupiter was expected to exhibit

active aurora potentially more energetic than the Earth's aurora. Jupiter's auroral emissions were observed at far-ultraviolet (FUV) wavelengths by the Voyager 1 Ultraviolet Spectrometer (UVS) in March 1979 (4), followed by spatially resolved spectra by the Earth-orbiting International Ultraviolet Explorer (IUE) in May 1979 (5). Jupiter's auroras have since been observed periodically by the IUE (6), and

other observations revealed thermal infrared (IR) hydrocarbon emissions (7), soft x-ray emissions (8), and near-IR ionospheric H_3^+ emissions (9). Images of the H_3^+ emissions reveal the main structures of the auroras at the limited angular resolution available from ground-based telescopes (10). High angular resolution images of the FUV auroral emissions have been obtained with the Hubble Space Telescope (HST) since 1990 (11, 12). Here we present a comprehensive analysis of the FUV auroral images taken by the HST Wide Field Planetary Camera 2 (WFPC2). These FUV images resulted from a decade-long program by the WFPC2 instrument development team (13) to produce alkali metal "Wood's" filters, which provide several times greater FUV sensitivity than earlier HST imaging while efficiently blocking visible light.

Observations and data reduction. FUV images of Jupiter were obtained with the HST WFPC2 between 19 May 1994 and 26 September 1995 (Table 1), including during the Comet Shoemaker/Levy 9 (S/L 9) impacts in July 1994. No effects of the S/L 9 impacts beyond those initially reported (12) have been found. The response of the WFPC2 with filter F160BW to an auroral spectrum includes the H_2 Lyman ($B^1\Sigma_u^+ - X^1\Sigma_g^+$) band emissions and part of the Werner ($C^1\Pi_u - X^1\Sigma_g^+$) band series plus the H Lyman α line (H-Ly α) (12). Inclusion of the F130LP filter blocks the H-Ly α emission and Werner bands: Such images were obtained in each observation to facil-

Table 1. WFPC2 FUV Images of Jupiter. Start time for first exposure, always at 17 s past the listed minute. Each observation consists of image pairs with filters F160BW and F160BW + F130LP in one HST orbit. Images with F160BW + F165LP were also obtained on 19 and 31 May 1994. CML are for midpoints of first and last exposure. Io orbital longitude, Io Orb.

Date	Start <i>t</i> (UT)	Exp. <i>t</i> (s)	CML (deg)	Io Orb. (deg)	Fig. 3	File name
5/19/94*	15:41	1500 × 2	199–247	27–37		u2eq0202
5/31/94	12:19	500, 600 × 2	74–92	279–283		u2eq0103
5/31/94	13:53	500, 600 × 2	131–149	292–296	H, K	u2eq0106
5/31/94	15:29	500, 600 × 2	189–207	306–310		u2eq0109
7/17/94	09:06	700 × 2	192–204	104–107	A	u2fi0e01
7/17/94	18:56	400 × 2	188–194	188–189	D	u2fi0j01
7/18/94	13:55	700, 800	158–170	341–343	E	u2fi0s01
7/19/94	11:07	400 × 2	205–211	160–162		u2fi0y01
7/20/94	14:10	400 × 2,	106–111	29–30		u2fi1501
		300 × 2	117–124	32–33	G	u2fi1503
7/20/94	16:12	400 × 2	176–182	47–48	F	u2fi1701
7/21/94	08:09	400 × 2	38–44	182–183	J	u2fi1b01
7/21/94	13:01	400 × 2	215–221	223–224		u2fi1f01
7/22/94	09:54	400 × 2	252–258	40–41		u2fi1p01
7/29/94†	08:57	700 × 2	192–205	16–18	I	u2fi7901
3/04/95†	23:10	600 × 2	6–17	179–181	L	u2fi0402
3/06/95†	20:15	600 × 2	201–212	201–203	C	u2fi0502
3/09/95†	17:25	700 × 2	190–202	67–69	B	u2fi0302
3/24/95†	14:28	700 × 2	182–193	214–217		u2fi0202
9/26/95†	09:35	500, 600	286–295	227–229		u2fi0102

*The first observation was 15 years to the day after the first IUE detection of Jupiter's aurora, and obtained with 2 × 2 binning on the CCD. †WF3 used, all others WF4. For WF4 the image of Jupiter was positioned in the corner opposite the pyramid apex; for WF3 it was centered on the CCD with the partially rotated filter position F160BN15.

J. T. Clarke and G. E. Ballester, Space Physics Research Laboratory, University of Michigan, Ann Arbor, MI 48109, USA.

J. Trauger, R. Evans, K. Stapelfeldt, D. Crisp, V. Meadows, Jet Propulsion Laboratory, Pasadena, CA 91109, USA.

J. E. P. Connerney, NASA Goddard Space Flight Center, Greenbelt, MD 20771, USA.

P. D. Feldman and R. E. Griffiths, Department of Physics and Astronomy, Johns Hopkins University, Baltimore, MD 21218, USA.

C. J. Burrows, S. Casertano, J. E. Krist, Space Telescope Science Institute, Baltimore, MD 21218, USA.

J. S. Gallagher III and J. G. Hoessel, Department of Astronomy, University of Wisconsin, Madison, WI 53706, USA.

J. J. Hester and P. A. Scowen, Department of Astronomy, Arizona State University, Tempe, AZ 85287, USA.

J. A. Holtzman and A. M. Watson, Department of Astronomy, New Mexico State University, Las Cruces, NM 88003, USA.

J. R. Mould, Mount Stromlo and Siding Springs Observatories, Australian National University, Weston Creek, ACT 2611, Australia.

J. A. Westphal, Division of Geological and Planetary Sciences, California Institute of Technology, Pasadena, CA 91125, USA.

*To whom correspondence should be addressed. E-mail: clarke@umich.edu

itate cosmic ray identification and to isolate the H-Ly α emission from the difference of images. Locations on Jupiter in the FUV images have been determined by an edge finding algorithm (12) and by comparison with a simulated disk reflection model. For the F160BW images we estimate positional uncertainties on Jupiter of ~ 300 -km projected area, comparable to the angular resolution. Jupiter's rotation results in image smear of about 1° of rotation per 100-s exposure time, degrading the resolution by the exposure length independently of the instrument resolution.

The images sample Jupiter's upper atmosphere over altitudes from the stratosphere to the thermosphere. In the FUV imaging bandpass of 1150 to 2100 Å, the altitude of line of sight optical depth unity ranges from 50-km altitude (0.1 bar pressure) at 2100 Å (determined by H₂ Rayleigh scattering) to 300 to 400 km (1 to 10 μ bar) below 1450 Å (from increasingly strong CH₄ photoabsorption) (14). The diffuse disk emission is dominated by scattered solar continuum over 1700 to 2100 Å, which has been modeled and subtracted to obtain accurate photometry of the aurora. Limb darkening has been modeled analytically using a Minnaert law formulation with empirical coefficients (15) for the F160BW bandpass. A mean latitudinal banding pattern has been derived from images taken on 31 May 1994 with filters F160BW + F165LP, which block the auroral emissions. The conversion to absolute brightness is based on mean WFPC2 sensitivity curves allowing for degradation with time after decontamination cycles (16).

Observed morphology of auroral emissions. Earlier HST images of Jupiter's northern aurora showed a main oval that appeared narrow at system III longitudes $\lambda > 180^\circ$ and broader at $\lambda < 180^\circ$. Little emission was detected from 270° to 110° , but variable small-scale features were seen along the oval with evidence for fainter emissions extending away from the oval (11, 17). With the higher WFPC2 sensitiv-

ity (18) and repeated imaging, it is now possible to distinguish the main emission structures of Jupiter's auroras. Persistent features at both poles include: (i) main auroral ovals with a similar longitude and latitude distribution on different days, although with large intensity variations along the ovals, (ii) patchy and variable emissions poleward of the main ovals and brightest at $\lambda < 180^\circ$, sometimes connected to and sometimes separated from the main oval, and (iii) discrete emission from the foot of Io's magnetic flux tube, always apparent when on the Earth-facing side of Jupiter. The emissions described in (ii) are seen more clearly in the north than in the south, and constitute a separate feature from the main oval spatially and in the sense that their brightness varies independently. Fainter emissions are often observed equatorward of the main oval (Fig. 1), but equatorward of the Io footprint locations (Fig. 4) upper limits with filter F160BW are about 10 kR (1 kilorayleigh = 10^9 photons $\text{cm}^{-2} \text{s}^{-1}$ into 4π steradians). This is at times less than 0.1% of the main oval emission, indicating a rapid decrease in emission at lower latitudes. A reported detection of FUV emission from the IFT footprint (19) is inconsistent with the observed location and brightness of this feature, while ground-based H₃⁺ emission features attributed to the IFT footprint (20) appear consistent with the WFPC2 locations.

The WFPC2 images at $\lambda > 180^\circ$ are similar to earlier Faint Object Camera (FOC) images of the north aurora (17), while the WFPC2 reference oval (21) is at a lower latitude ($\lambda < 180^\circ$). The emissions at $\lambda < 180^\circ$ are variable and near the diffuse emission poleward of the main oval. Due to their lower sensitivity, the FOC images might have detected the auroral emission poleward of the main oval without resolving distinct emission from the main oval. The WFPC2 ovals are also consistent with the auroral oval locations derived from

ground-based H₃⁺ images (22). Comparison of WFPC2 images with Voyager UVS observations of the equatorward extent of the northern aurora (23), shows that the WFPC2 ovals are similar near 180° , but near 0° longitude the UVS oval extends to much lower latitudes. The UVS may have detected fainter emissions than WFPC2, being sensitive to emissions of a few hundred rayleighs. Emissions appearing above the limb (as seen by WFPC2) might also have been assigned to the latitude of the apparent limb. The overall emission pattern co-rotates with Jupiter's magnetic field except the IFT "footprint," which always appears close to the foot of Io's magnetic flux tube. The fixed nature of the IFT footprint is striking in the series of images on 31 May 1994 covering 133° of jovian rotation (24), providing a detection of FUV emission from the IFT footprint and unambiguously identifying this feature with Io.

Fig. 1. WFPC2 F160BW image of Jupiter on 24 March 1995 showing three main features of auroral emission discussed in text: The Io footprint emission appears on the equatorward right side of the main oval north and south. The result of modeling and subtracting the long wavelength disk component is shown on the right, revealing no detectable emission equatorward of the locus of observed Io footprint emissions.

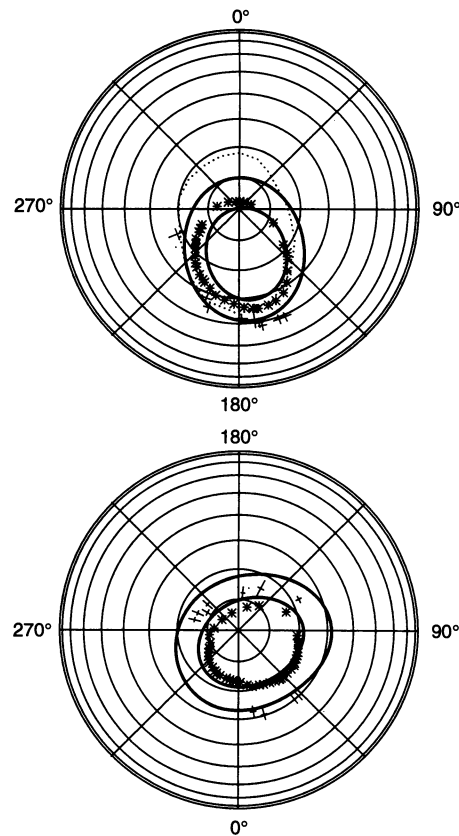
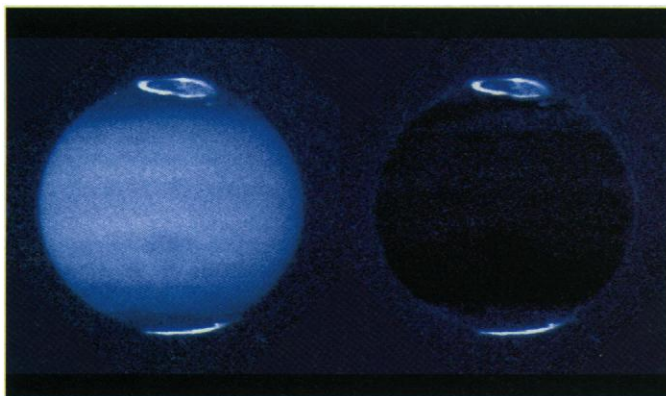


Fig. 2. Polar projections showing the "WFPC2" reference auroral ovals (asterisks) from March 1995 overplotted with the locations of the 6 (outer) and 30 (inner) R_J ovals in the O_6 model with current sheet (solid lines) and the Voyager UVS oval (dashed). Top projection shows northern hemisphere and bottom projection shows southern hemisphere. The regions with few points are regions appearing near the limb and therefore more uncertain. "Plus" marks indicate the location of Io footprint emissions, with the lengths of the lines indicating positional uncertainties.

There is a high degree of variability in the auroral morphology (Fig. 3). Emissions are observed from both poles at all longitudes, indicating that at least part of the auroral "curtain" is always visible over the limb (25). The limb observing geometry precludes a unique determination of the spatial distribution, while the large slant path through the auroral curtain produces a brightness enhancement along the main oval. The emissions always extend clearly above the planetary limb, and modeled ovals with assumed base altitudes of 400 to 700 km give good fits to the observed emissions. Part of the observed brightening from the far side of the main oval may be limb brightening from diffuse emission near the limit of detection inside the main oval. The diffuse emissions poleward of the oval range from near the limit of detection to as bright as 700 kR. An estimate of the auroral color ratio (26) from a comparison of the F160BW and F160BW + F130LP images indicates that the IFT footprint has a similar color ratio to the main oval, while the diffuse emission is significantly brighter at shorter wavelengths, indicating softer particles and/or emission at higher altitudes. For a typical (300 kR) and the brightest (3 MR) emissions observed along the main oval (assuming 10% radiative efficiency), the local energy dissipation in Jupiter's atmosphere is 45 to 450 $\text{erg cm}^{-2} \text{s}^{-1}$. Energy deposition of this magnitude will produce a local supersonic expansion from Joule heating and likely runaway currents in the ionosphere, with an auroral electrojet potentially stronger than on the Earth. The observed radiated power in the north in images with central meridian longitudes (CML) near 180° ranges over a few times 10^{11} to 10^{12} W, with a corresponding input power about 10 times larger. As expected (27), the auroral energy input dominates over the global, solar FUV input to Jupiter's thermosphere.

Mapping auroral emission features into

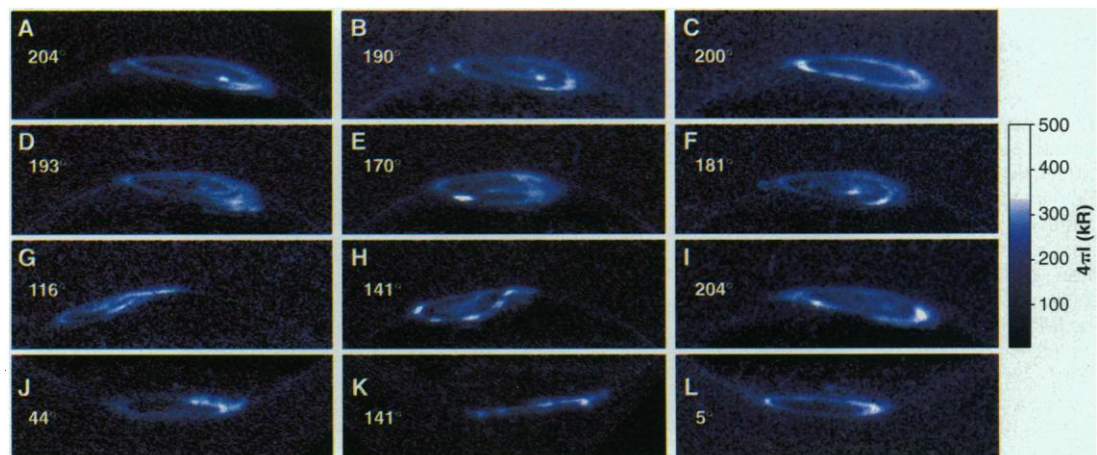
Jupiter's magnetosphere. The auroral emission locations can constrain the magnetospheric regions where precipitating charged particles originate, if the magnetic field can be accurately mapped (28). Since the main oval always appears poleward of the Io footprint emission, the main auroral processes must occur farther from Jupiter than Io's orbit without regard to any planetary magnetic field model. This contradicts the Voyager era view (23) that the FUV aurora were associated with the Io torus, and it is based on the simultaneous detection of the Io footprint and main oval. From the observed 4° to 6° latitude difference, we estimate that the main oval maps to equatorial regions greater than 12 jovian radii (R_J) from Jupiter. This is consistent with the outer half of the co-rotation portion of Jupiter's middle magnetosphere, where there is a large magnetic distortion due to the co-rotating magnetodisc current. The local field is almost radial near the magnetodisc, making it difficult to map from the auroral zone to a unique equatorial distance. By contrast, the Io footprint emissions originate from an electric current tied to Io at a known location, sufficiently close that the planetary field dominates over the current sheet. While the footprint emission may deviate from Io's instantaneous field line in longitude, no significant deviation in latitude is expected. The observed latitude differences are up to 6°, within the 10° uncertainty in the O_6 model (28), and the observed Io footprint emissions can be used to more accurately map the field near Jupiter. The observed auroral ovals (Fig. 2) lie between the modeled 6 R_J and 30 R_J (29) ovals in the north and poleward of the 30 R_J oval in the south, with some deviations from the model ovals at both poles. Much of this deviation is due to the uncertainty in the O_6 model of Jupiter's higher order magnetic moments, which dominate the field geometry near the planet.

Jupiter's aurora are evidently unlike the

Earth's aurora. The region of maximum likelihood of auroral emission on the Earth consists of a pattern which is fixed with respect to the solar wind direction, under which the planet rotates. This statistical auroral oval shifts with respect to the surface as the Earth rotates, and the auroral emission is enhanced on the night side where the statistical oval is broader than on the day side. By contrast, Jupiter's overall emission pattern (except the Io footprint) rotates nearly fixed in magnetic longitude and latitude, while intensity changes and relative motions occur along each oval. This is seen in images covering 40% of a jovian rotation on 31 May 1994 (24), with bright emissions moving across the day and night sides in the north and south, as well as in 36 other images over 1½ years (Fig. 3). Jupiter's co-rotating auroral pattern is consistent with our expectation that the magnetosphere is energetically driven by the planet's rotation, in contrast with the Earth's extraction of power from the solar wind.

The width of Jupiter's main oval varies with location and time (Fig. 3). For northern images with CML near 180°, the morning portion of the oval often appears narrow, while the afternoon section appears broken in latitude and sometimes merges with the poleward emissions (17). The region of broken emissions appears confined to $\lambda \sim 140^\circ$ to 180° (the region of strongest northern magnetic field). The large number of observations with CML = 150° to 200° (chosen for optimal viewing of the northern aurora) presents a selection effect, since it places the $\lambda \sim 140^\circ$ to 180° preferentially in the noon or afternoon sectors. Additional repeated images during a single Jupiter rotation will be needed to distinguish between magnetic local time effects and longitudinal asymmetries. In addition, the observed main oval emissions (Fig. 3, C and L) follow the WFPC2 reference ovals, whereas significant deviations from the ref-

Fig. 3. Montage of F160BW images when Jupiter's north or south (J, K, and L) magnetic pole was tilted toward the Earth for good viewing of the aurora with an intensity scale in kilorayleighs. Numbers indicate the longitude of the central meridian at the midpoint of each exposure. Auroral emissions appear at both poles in each image, although only one pole is shown here for brevity. Note the changing location of the main oval with respect to the reference ovals (dotted lines) and changes in the emission within the oval.



erence ovals occur in other images taken at similar CML's. Most of these deviations occur over $\lambda \sim 10^\circ$ to 180° . One unusual image (Fig. 3D), shows an incomplete oval with dusk sector emissions covering latitudes mapping from about $6 R_J$ to the distant magnetosphere in a series of nearly parallel arcs.

The broken main oval at times appears to merge with the diffuse emissions poleward of the oval, concentrated at $\lambda < 180^\circ$. The poleward emissions run generally parallel to the main oval, at times resembling the Earth's "theta aurora" pattern of a linear feature across the oval. By contrast, we have not observed Jupiter's diffuse emission to connect opposite sides of the main oval, nor has it been observed to follow the local noon-midnight direction. We therefore expect that it is produced by a different process than the Earth's theta aurora. Jupiter's poleward emissions may connect to regions in the outer magnetosphere where the plasma flow is radially outward, and thereby represent an Earth-like auroral process driven by magnetospheric convection, compared with the main oval driven by partial co-rotation of the middle magnetosphere. Another possibility is that they may be produced by an ionospheric current system in the polar cap driven by heating in the main oval.

The images on 31 May 1994 show a rapidly changing auroral morphology as Jupiter rotated, with an auroral storm developing near the dawn limb (24), similar to outbursts observed in the past (30). The repeated appearance of bright storms near the dawn limb suggests that there is also some local time dependence of the auroral activity. A likely factor in any local time changes in Jupiter's aurora would be the plasma flow pattern in Jupiter's middle magnetosphere (31). With an internal plasma source at Io, Jupiter's rapid rotation and the solar wind pressure combine to produce a net outward plasma flow in the afternoon and night sectors, changing to a compression and inward flow in the pre-dawn and morning sectors for the co-rotating plasma. Theories predict strong particle acceleration and partial co-rotation of plasma structures in the dawn sector (31), and the afternoon relaxation of the plasma might result in the more diffuse and broken auroral structures.

In those images showing north and south auroral ovals, there also appears to be a high degree of north and south magnetic symmetry in the emission features. Not knowing the structure of the current sheet, there is a large uncertainty in the magnetic field tracing of these features. However, features that appear conjugate between the north and south auroras appear consistent with the opposite ends of the same $30 R_J$ field lines within the uncertainty in the O_6

model. We have seen no examples of bright features at one pole that do not have conjugate features at the other pole. The observed conjugacy has implications for the nature of the process(es) by which charged particles are accelerated and scattered into the loss cone. For example, earlier suggestions (32) that ions and electrons drift in opposite directions (east or west) until entering the loss cone predicted bright aurora at specific longitudes which differ between the north and south, and this pattern has not been observed.

The Io flux tube "footprint" aurora. Io is electrically conducting by virtue of its ionosphere, with Jupiter's magnetic field and the co-rotating plasma torus sweeping past at a speed exceeding Io's orbital motion by 56 km s^{-1} . Following early decametric observations, a continuous electric current linking Io with Jupiter's ionosphere was proposed, driven by Io acting as a unipolar inductor with a 400-kV potential (34) across its diameter radially away from Jupiter (3). The Voyager 1 spacecraft passed about 20,000 km south of Io, and found the local magnetic field and plasma flow distorted by a $3 \times 10^6 \text{ A}$ field-aligned current (33) along Io's magnetic flux tube. The existence of the plasma torus along Io's orbit implied that the field-aligned current would be carried by Alfvén waves propagating at a speed determined by the local plasma density (34). The measured torus plasma density suggested that the Alfvén waves carrying the current should return from Jupiter's ionosphere after Io had passed beyond those magnetic field lines (34), so that the circuit would not maintain a direct current structure. The IFT "footprint" auroral emission that we observe is produced by currents in and out of Jupiter's upper atmosphere. The integrated propagation time and path along the magnetic field between Io and Jupiter correspond to the emission leading the undisturbed magnetic footprint, since the co-rotation of the field exceeds Io's orbital motion, in the same direction as the deviation proposed in the direct current model (3). Jupiter's rotation with an inclined and asymmetric magnetic field causes the torus to move north and south with respect to Io, thereby varying the current path length through the torus with longitude (in the opposite sense north and south), and the field strength (and corresponding electric potential) at Io varies by 20% with longitude (34). These factors suggest that we might observe variations in the location and brightness of the IFT footprint aurora with sub-Io longitude.

The centers of light of the footprint auroral emissions with respect to the instantaneous undisturbed magnetic footprint of Io (28) (Fig. 4) indicate a trend toward the

emission leading by 0 to 10° , with maximum lead angles for the southern emissions near 180° longitude (with Io near the northern edge of the torus) and minimum near 0 to 50° longitude (Io near the southern edge of the torus). The lead angle might correspond to the travel delay determined by the integrated density of plasma along the current path, also consistent with the northern lead angle being near zero at 180° longitude. Note, however, that the observed footprint emission often deviates from the O_6 model magnetic footprint by up to 6° in latitude and longitude. The leads in longitude (Fig. 4) could simply reflect the inaccuracy of the field model.

Io's footprint emission has a central bright region with diffuse fainter emission extended in longitude (Fig. 5). This fainter emission is near the sensitivity limit, suggesting that the emission may be more extended than observed. The integrated brightnesses over 0.5-arc sec areas range over a factor of 4, decreasing to a factor of 2 after correcting for an assumed cosine limb brightening for the optically thin emission. Beyond the factor of 2 intrinsic variability, we find no systematic depen-

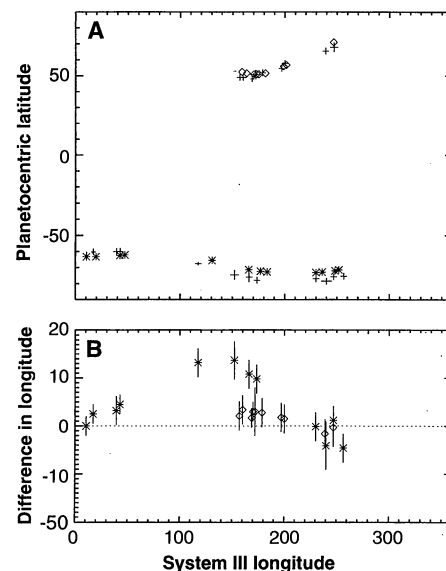


Fig. 4. (A) The observed locations of Io footprint emissions are given by plus signs (with positional uncertainty indicated by length of lines) and compared with instantaneous magnetic field footprints (28) with diamonds for northern points and asterisks for southern points. (B) The difference in longitude, given as a lead or lag in the co-rotation direction, from each observation is plotted with error bars indicating only the positional uncertainty in the observed locations. The additional uncertainty in the magnetic field model appears to be $\sim 6^\circ$. These plots include only the observations where the Io footprint appeared sufficiently far from Jupiter's limb that an accurate position could be determined. Units for all axes are given in degrees.

dence of the brightness with longitude, as expected for a varying flux tube current north to south and varying jovian ionospheric conductivity with longitude. For the brightest emissions, an average of 120 kR over a 0.5-arc sec area requires nearly 10^{11} W input power. This is a significant fraction of the total power in the circuit, estimated as a maximum of 1.2×10^{12} W for 3×10^6 A current and a 400-kV potential across Io's diameter, implying a strong dissipation of the current in Jupiter's ionosphere.

An extended emission was seen in July 1994, extending several tens of degrees east and west (Fig. 3A). The extension is visible in part due to limb brightening and the foreshortened geometry near the limb, however in another observation with a similar geometry and longer exposure (Fig. 3B) no such extension was observed. A similar extension of the IFT footprint H_3^+ emission with longitude has been reported for IR observations in July 1995 (36). The extension to decreasing longitude is con-

sistent with reflecting Alfvén wave propagation, for which there is independent evidence in the decametric radio emissions (37). The extension to greater longitudes is presently unexplained. A remarkable aspect of the current loop between Io and Jupiter is the correspondence between the 60- to 120-kR auroral emissions from the footprint on Jupiter and the 10-kR FUV emissions produced in Io's atmosphere. Taking into account the relative areas of the emissions at Io and Jupiter, the energy dissipated as FUV radiation is only about two times greater at Jupiter than in Io's airglow, with the larger area of emission at Io compensating for the lower surface brightness. Caveats to this include the presently unknown contribution to Io's emission from impacting torus plasma, the relative efficiencies of emission production in the different atmospheres, and the role of field-aligned potentials. The general agreement of the dissipated energies, coupled with the fairly constant footprint brightness, provide sup-

porting evidence for dissipation of a relatively stable current system between the ionospheres of Jupiter and Io. Measurement of the magnetic field perturbation near Io by the Galileo magnetometer has led to the suggestion that Io has an intrinsic magnetic field aligned parallel to Jupiter's field near Io (39). This may be consistent with our observation that the Io footprint emission varies relatively little in brightness with time or sub-Io longitude. The local energy dissipation in Jupiter's atmosphere is $30 \text{ erg cm}^{-2} \text{ s}^{-1}$ for a 200-kR emission in the brightest pixel, which again will strongly disturb the local ionosphere and neutral atmosphere for a short time as the feature moves past. Finally, the footprint emissions are resolved in these images, extending in longitude and latitude beyond the smearing determined by the changing magnetic mapping of Io during each exposure (39). The magnetic field outlining Io's diameter projects to a width of the order of 200 km at Jupiter's atmosphere, while the emission full width at half maximum is roughly 1000 to 2000 km after correction for rotational smearing (Fig. 5).

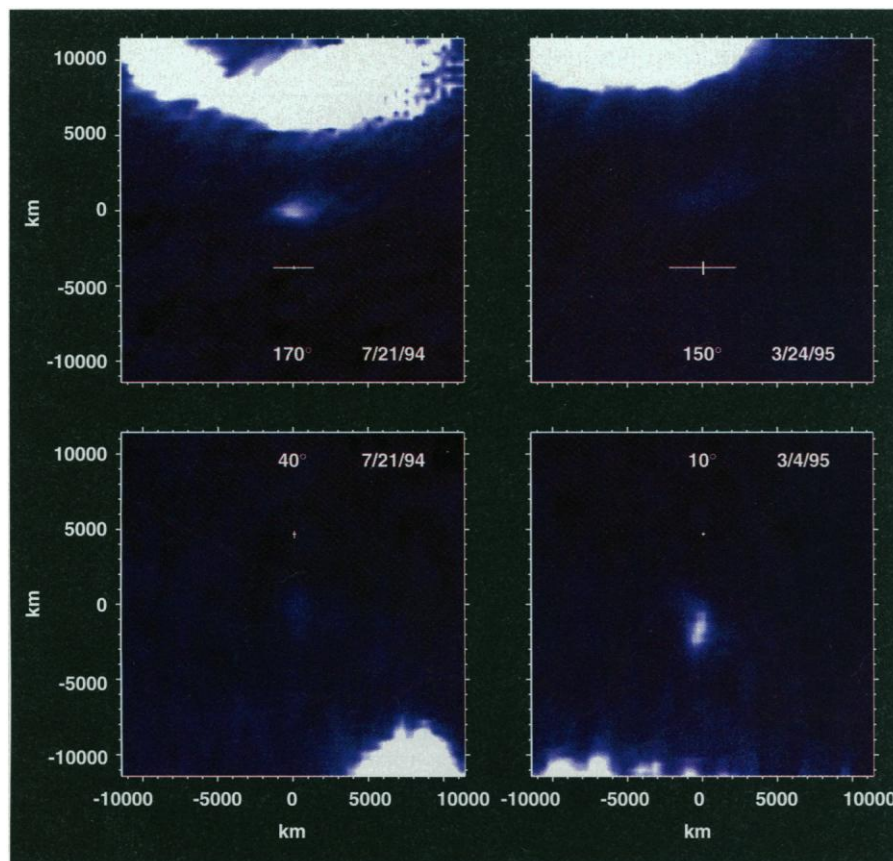


Fig. 5. Images backprojected to a view looking straight down on the Io footprint emissions (center of each frame) with distance in kilometers, showing the extended nature and changing morphology of the footprint emission. The longitude indicated in each frame corresponds to the sub-Io longitude during the exposure. Upper panels show the northern aurora and lower panels show the southern aurora. White error bars in each frame indicate the apparent motion of Io's magnetic flux tube during the exposure (calculated from the O_3 field model). This motion is mainly due to the changing magnetic field geometry rather than Io's orbital motion. The more extended appearance in the upper images is largely due to greater longitudinal motion of the flux tube during those exposures.

REFERENCES AND NOTES

- B. F. Burke and K. L. Franklin, *J. Geophys. Res.* **60**, 213 (1955).
- E. K. Bigg, *Nature* **203**, 1008 (1964).
- J. H. Piddington and J. F. Drake, *ibid.* **217**, 935 (1968); P. Goldreich and D. Lynden-Bell, *Astrophys. J.* **156**, 59 (1969).
- A. L. Broadfoot *et al.*, *Science* **204**, 979 (1979).
- J. T. Clarke *et al.*, *Astrophys. J. Lett.* **241**, L179 (1980).
- T. E. Skinner *et al.*, *Astrophys. J.* **278**, 441 (1984); T. A. Livengood *et al.*, *Icarus* **97**, 26 (1992); W. M. Harris *et al.*, *ibid.*, in press.
- T. Kostiuik *et al.*, *Infrared Phys.* **1**, 431 (1977); J. Caldwell, A. T. Tokunaga, F. C. Gillett, *Icarus* **44**, 667 (1980); P. Drossart *et al.*, *ibid.* **66**, 610 (1986); J. Caldwell *et al.*, *ibid.* **74**, 331 (1988).
- A. Metzger *et al.*, *J. Geophys. Res.* **88**, 7731 (1983); J. H. Waite *et al.*, *ibid.* **99**, 14799 (1994).
- P. Drossart *et al.*, *Nature* **340**, 539 (1989); L. Trafton, D. F. Lester, K. L. Thompson, *Astrophys. J. Lett.* **343**, L73 (1989).
- S. J. Kim *et al.*, *Nature* **353**, 536 (1991); R. Baron *et al.*, *ibid.*, p. 539.
- J. Caldwell *et al.*, *Science* **257**, 1512 (1992); V. Dols *et al.*, *Geophys. Res. Lett.* **19**, 1803 (1992); J. C. Gérard, V. Dols, F. Paresce, R. Prangé, *J. Geophys. Res.* **98**, 18793 (1993).
- J. T. Clarke *et al.*, *Science* **267**, 1302 (1995).
- J. T. Trauger *et al.*, *Astrophys. J. Lett.* **435**, L3 (1994); J. Holtzman *et al.*, *Pub. Astron. Soc. Pac.* **107**, 156 (1995); J. T. Clarke *et al.*, in *Calibrating Hubble Space Telescope Post Servicing Mission*, A. Koratkar and C. Leitherer, Eds. (Space Telescope Science Institute, Baltimore, MD, 1995) pp. 322-333.
- The effective wavelength in the FUV images is estimated by convolving an IUE spectrum of Jupiter with the WFPC2 instrument response.
- R. A. West *et al.*, *Science* **267**, 1296 (1995).
- Brightnesses are estimated in each bandpass using average sensitivity values of 0.00057 and 0.00050 electrons per second per WF pixel for 1-kR emissions with F160BW and F160BW + F130LP, and a sensitivity degradation of 40% in 30 days after each decontamination.
- J. C. Gérard, V. Dols, R. Prangé, F. Paresce,

- Planet. Space Sci.* **42**, 905 (1994); D. Grodent, V. Dols, J. C. Gérard, *J. Geophys. Res.* **101**, 2163 (1996).
18. Intensity traces across Jupiter's polar regions in closely spaced WFPC2 and FOC images in July 1994 give three times higher sensitivity to the auroral spectrum with WFPC2. The main oval also appeared narrower in the FOC images due in part to the higher threshold of detection.
 19. S. K. Atreya, Y. L. Yung, T. M. Donahue, E. S. Barker, *Astrophys. J. Lett.* **218**, L83 (1977); A revised flux calibration [E. S. Barker *et al.*, *Astrophys. J.* **242**, 383 (1980)] requires the IFT footprint emission reported by Atreya *et al.* to have been more than 1 MR (an order of magnitude brighter than observed by HST WFPC2), and the aperture locations at the three times of detection would not have included the IFT footprint from the locus of points in Fig. 2. The reported detections, if real, are likely to have been emission from the main oval, which was not considered.
 20. J. E. P. Connerney *et al.*, *Science* **262**, 1035 (1993).
 21. WFPC2 reference ovals were created from images showing complete ovals on 24 March 1995 (north) and 4 March 1995 (south). These are reference ovals, not statistical or maximum likelihood ovals, and were established as a basis for comparison with other images.
 22. P. Drossart, R. Prangé, J.-P. Maillard, *Icarus* **97**, 10 (1992); Y. H. Kim, S. J. Kim, J. A. Stuewe, J. Caldwell, T. M. Herbst, *ibid.* **112**, 326 (1994); J. E. P. Connerney, T. Satoh, R. L. Baron, *ibid.* **122**, 24 (1996).
 23. A. L. Broadfoot, *et al.*, *J. Geophys. Res.* **86**, 8259 (1981).
 24. G. E. Ballester *et al.*, *Science* **274**, 409 (1996).
 25. The wavelength dependent geometric distortion created a prism dispersion of the auroral spectrum, up to a few pixels over the south pole, in all WF4 images. With a partially rotated filter on WF3 (available after 29 July 1994) this dispersion is negligible.
 26. The auroral color ratio of H₂ emissions (1557 to 1619 Å) to (1230 to 1300 Å) indicates the degree of CH₄ photoabsorption (strong below 1450 Å) and corresponding atmospheric column above the auroral emissions, defined by Y. L. Yung, G. R. Gladstone, K. M. Chang, J. M. Ajello, and S. K. Srivastava [*Astrophys. J. Lett.* **254**, L65 (1982)].
 27. J. T. Clarke, J. Caldwell, T. Skinner, R. Yelle, *NASA Spec. Pub.* **494** (1989) p. 211.
 28. J. E. P. Connerney, in *Planetary Radio Emission III*, H. Rucker, M. L. Kaiser, S. J. Bauer, Eds. (Austrian Academy of Science Press, Vienna, 1992), p. 13. O₆ magnetic field estimates include Jupiter's intrinsic field and a current sheet appropriate to the time of Voyager 1 encounter, derived from in situ measurements by the Pioneer and Voyager spacecraft.
 29. Auroral ovals are quoted in units of R_J referring to the distance at which the field lines cross the projected equator.
 30. T. A. Livengood, H. W. Moos, G. E. Ballester, R. Prangé, *Icarus* **97**, 26 (1992); R. Prangé *et al.*, *J. Geophys. Res.* **98**, 18779 (1993); J. C. Gérard *et al.*, *Science* **266**, 1675 (1994).
 31. V. M. Vasylunas, in *Physics of the Jovian Magnetosphere*, A. J. Dessler, Ed. (Cambridge Univ. Press, Cambridge, 1983), p. 395; D. D. Barbosa, *Planet. Space Sci.* **35**, 119 (1987).
 32. R. Prangé and M. Elkhamsi, *J. Geophys. Res.* **96**, 21371 (1991).
 33. M. H. Acuna, F. M. Neubauer, N. F. Ness, *ibid.* **86**, 8513 (1981).
 34. F. M. Neubauer, *ibid.* **85**, 1171 (1980); J. W. Belcher, *Science* **238**, 170 (1987).
 35. The identification of emissions with Io's magnetic footprint results from observing the emissions following Io's orbital motion, as well as their detection near the IFT footprint in ~20 separate WFPC2 images. The single detection and three non-detections by FOC from July 1994, reported by R. Prangé *et al.*, *Nature* **379**, 323 (1996), do not by themselves identify the feature with the IFT footprint, although when combined with the WFPC2 data and the lower FOC sensitivity this appears likely to have been footprint emission. The lead angles derived from H₃⁺ footprint emissions (21) appear systematically larger than those reported here, a difference that is presently unresolved.
 36. J. E. P. Connerney *et al.*, *Bull. Am. Astron. Soc.* **27**, 1147 (1995).
 37. Y. Leblanc, G. A. Dulk, F. Bagenal, *Astron. Astrophys.* **290**, 660 (1994).
 38. M. G. Kivelson *et al.*, *Science* **274**, 396 (1996).
 39. The IFT footprint moves in both latitude and longitude over the course of each exposure, depending on the magnetic field mapping over time. The estimated smearing of the footprint from the expected locations in the O₆ model at the beginning and end of each exposure has been subtracted from the observed emission full width at half maximum to estimate the intrinsic width.
 40. We acknowledge helpful conversations with J. Belcher, M. Kivelson, F. Bagenal, and F. Crary. This work is based on observations with the NASA/ESA Hubble Space Telescope, obtained at the Space Telescope Science Institute (STScI), which is operated by the AURA, Inc. for NASA under contract NASS-26555. The research was supported by contract JPL 959122 from NASA's Jet Propulsion Laboratory and grant GO-5624.18-93A from the Space Telescope Science Institute to the University of Michigan.

3 July 1996; accepted 26 September 1996

Time-Resolved Observations of Jupiter's Far-Ultraviolet Aurora

Gilda E. Ballester,* John T. Clarke, John T. Trauger, Walter M. Harris, Karl R. Stapelfeldt, David Crisp, Robin W. Evans, Eric B. Burgh, Christopher J. Burrows, Stefano Casertano, John S. Gallagher III, Richard E. Griffiths, J. Jeff Hester, John G. Hoessel, Jon A. Holtzman, John E. Krist, Vikki Meadows, Jeremy R. Mould, Raghvendra Sahai, Paul A. Scowen, Alan M. Watson, James A. Westphal

Simultaneous imaging and spectroscopic observations of Jupiter's far-ultraviolet aurora covering half a jovian rotation were made on 31 May 1994. The Hubble Space Telescope Wide Field Planetary Camera 2 images revealed dramatic and rapidly changing auroral features, including discrete longitudinal structures along the auroral ovals, with variable contrast; a poleward offset in a north oval sector, showing equatorward motion near dusk; emissions polewards of the ovals, apparently co-rotating; and a bright event developing near the dawn limb. Viewing geometry effects explain the rotational intensity modulation observed by the International Ultraviolet Explorer, without intrinsic longitudinal asymmetries.

The first decade of studies of Jupiter's aurora in far-ultraviolet (FUV) H Lyman α (H-Ly α) and H₂ emissions by the Voyager spacecraft (1) and the International Ultra-

violet Explorer (IUE) (2) emphasized the north aurora. These data were fitted by a low-latitude oval (reaching +60° latitude) mapping along the magnetic field lines out to the Io plasma torus at 6 jovian radii (R_J), and with an enhanced emission region fixed around magnetic System III longitude $\lambda \sim 180^\circ$ to 210° contributing to the observed rotational modulation. This interpretation suggested jovian auroral processes quite different than those on Earth, with longitudinal dependencies related to large asymmetries in Jupiter's co-rotating surface magnetic field, and associated with the torus and the inner magnetosphere. These magnetospheric regions are dominated by a co-rotating equatorial plasma sheet supplied by the torus and extending tens of jovian radii into the middle magnetosphere (3). Remote images of the FUV aurora obtained with the Faint Object Camera (FOC) (4) and the Wide Field Planetary Camera 2 (WFPC2) (5, 6) on the Hubble Space Telescope (HST) are now revealing a different picture. They show high-latitude emissions mapping to the middle magnetosphere,

G. E. Ballester and J. T. Clarke, Space Physics Research Laboratory, University of Michigan, Ann Arbor, MI 48109, USA.

J. T. Trauger, K. R. Stapelfeldt, D. Crisp, R. W. Evans, V. Meadows, R. Sahai, Jet Propulsion Laboratory, Pasadena, CA 91109, USA.

W. M. Harris, J. S. Gallagher III, J. G. Hoessel, Department of Astronomy, University of Wisconsin, Madison, WI 53706, USA.

E. B. Burgh, C. J. Burrows, R. E. Griffiths, Department of Physics and Astronomy, Johns Hopkins University, Baltimore, MD 21218, USA.

S. Casertano and J. E. Krist, Space Telescope Science Institute, Baltimore, MD 21218, USA.

J. J. Hester and P. A. Scowen, Department of Astronomy, Arizona State University, Tempe, AZ 85287, USA.

J. A. Holtzman and A. M. Watson, Department of Astronomy, New Mexico State University, Las Cruces, NM 88003, USA.

J. R. Mould, Mount Stromlo and Siding Springs Observatories, Australian National University, Weston Creek, ACT 2611, Australia.

J. A. Westphal, Division of Geological and Planetary Sciences, California Institute of Technology, Pasadena, CA 91125, USA.

*To whom correspondence should be addressed. E-mail: gilda@umich.edu